Journal of Molecular Spectroscopy 296 (2014) 1–8

Contents lists available at ScienceDirect

Journal of Molecular Spectroscopy

journal homepage: www.elsevier.com/locate/jms

High-resolution infrared spectra of vibrationally excited HC_4H in a supersonic hydrocarbon plasma jet

Dongfeng Zhao *, Kirstin D. Doney, Harold Linnartz

Sackler Laboratory for Astrophysics, Leiden Observatory, University of Leiden, PO Box 9513, NL 2300 RA, Leiden, The Netherlands

ARTICLE INFO

Article history:
Received 5 October 2013
In revised form 22 November 2013
Available online 8 December 2013

Keywords:
Infrared spectroscopy
Vibrationally excited diacetylene
cw-CRDS
Supersonic plasma jet

ABSTRACT

High-resolution infrared spectra of diacetylene (HC_4H) are recorded in the 3 μm C—H stretch region using continuous wave cavity ring-down spectroscopy (cw-CRDS). The HC_4H molecules are generated in a pulsed and supersonic planar plasma expansion by discharging a C_2H_2/He/Ar gas mixture. The jet-cooling realizes a low rotational temperature of $T_{rot} \sim 17$ K. Vibrational temperatures are found to be relatively high, allowing the detection of vibrationally excited HC_4H in direct absorption with energies up to 1800 cm^{-1}. In total, sixteen ro-vibrational bands are identified, where nine of them were not reported before. Detailed and systematic rotational analyses are presented, yielding spectroscopic parameters for a series of vibrational levels over energy regions of 0–1800 and 3300–5100 cm^{-1}. Using the observed infrared band intensities, two vibrational excitation temperatures of HC_4H in the plasma jet, ~570(50) K for the v_6, v_7 and v_8 bending vibrations, and ~125(10) K for the v_9 bending vibration, are deduced.

1. Introduction

As a substantial reservoir of carbon in the universe, unsaturated hydrocarbons and their derivatives are important constituents in common reaction schemes [1]. Among them, highly unsaturated (poly)acetylenes of the form of $HC_{2n}H$, are commonly involved in combustion chemistry [2,3], plasma processing [4,5], chemical syntheses and material sciences [6–9], Due to their unstable and highly reactive nature, they also play an important role in the chemical evolution of planet atmospheres and in the chemistry of the interstellar medium (ISM) [10–14]. In astrochemical models, acetylene, diacetylene and derivatives, including the cyano derivatives HCN and HC_3N, are thought to link known gas-phase molecules and complex organics. Since diacetylene is photochemically reactive [15–20], photolysis of diacetylene can result in the production of longer carbon-chain species, such as tri- (HC_6H) and tetra-acetylene (HC_8H). Although not conclusively proven yet, acetylene and diacetylene are believed to be important intermediates in the reaction scheme leading to the formation of large organic molecules that make up the "haze" of the atmospheres of gas giant planets [10,11,17,21].

Small polyacetylenes, primarily diacetylene (HC_4H), have been identified in many carbon-rich atmospheres of planets and their moons. In 1981, diacetylene was identified for the first time in space in the atmosphere of Titan, by Voyager's infrared interferometer spectrometer (IRIS) [22]. In 1997, diacetylene was identified again in Infrared Space Observatory (ISO) spectra from Saturn [23], which led to the suggestion that small polyacetylenes are involved in giant planet atmospheric chemistry [14,24]. In 2004, following the predictions of photochemical models [25,26], diacetylene was detected in the atmospheres of Jupiter [27], and the remaining giant planets Uranus [28] and Neptune [29]. In the interstellar medium (ISM), detection of small polyacetylenes has been accessed in two carbon-rich protoplanetary nebulae, CRL 618 and CRL 2688 [30–32], in Spitzer infrared observations against the dust shell of a nova like star V4334 Sgr [33], as well as in the extragalactic Large Magellanic cloud (LMC) [34].

Due to the lack of a permanent dipole moment, diacetylene cannot be detected by rotational transitions in the microwave region, and therefore ro-vibrational spectra in the infrared and submillimeter-wave region are the most important spectroscopic tools to detect HC_4H both in the laboratory and in astronomical observations [20–24,30–36]. For example, detections of diacetylene in planetary atmospheres are mainly via the strong perpendicular band v_8, at 627.9 cm^{-1} [23,27–29], and in the protoplanetary nebulae of CRL 618 and CRL 2688 via the parallel combination band $v_6 + v_8$, at 1241 cm^{-1} [30–32].

In the past few decades, series of high-resolution laboratory spectroscopic studies on diacetylene have been reported with spectral coverage ranging from submillimeter-wave to infrared [35–47]. These measurements were generally performed at room temperature with pure diacetylene gas samples synthesized in the laboratory, resulting in accurate spectroscopic parameters for a number of low-lying vibrational levels. These room-temperature spectra, particularly the spectrum in the C—H stretch region at

* Corresponding author.
E-mail address: zhao@strw.leidenuniv.nl (D. Zhao).

0022-2852/$ - see front matter © 2013 Elsevier Inc. All rights reserved.
http://dx.doi.org/10.1016/j.jms.2013.11.008

~3 μm [38], suffer heavily from spectral blending, and Doppler broadened line profiles which prohibit detailed analysis of weak absorption features, such as low-*J* transitions and weak vibrational hot bands. Recently, we demonstrated a new laboratory approach that allows to record high-resolution infrared spectra of hydrocarbons in pulsed supersonic planar plasma [48]. It was found that the jet-cooling results in a low rotational temperature of HC_4H and simplifies the experimental spectra. A sensitive cavity ring-down detection scheme allows us to detect the low-*J* transitions of a series of weak hot bands. In this work, we present a detailed analysis of the ro-vibrational transition band system of HC_4H in the 3306–3342 cm^{-1} region. Chemical formation and the non-equilibrium relaxation of vibrationally excited HC_4H in a supersonic plasma jet are also discussed based on the experimental findings.

2. Experiment

The experimental setup has been described in detail recently [48]. Diacetylene molecules are produced in a pulsed supersonic planar plasma jet by discharging 0.5% C_2H_2 diluted in a He/Ar ~1:1 gas mixture. A gas pulse (~1 ms), with a typical backing pressure of ~15 bar, is supersonically expanded into a vacuum chamber through a pulsed valve (General Valve, Series 9, 2 mm orifice) that is mounted on top of a 3 cm × 0.3 mm multi-layer slit discharge nozzle. The vacuum chamber is evacuated by a roots blower pump station (4800 m^3/h). Typical discharge V/I values are ~−1200 V/50 mA. The discharge nozzle is aligned with its slit throat in parallel to and ~5 mm away from the optical axis of a high finesse cavity which is used for cavity ring-down measurements. The cavity is 56 cm long and comprises two highly reflective plano-concave mirrors (1 m radius of curvature, reflectivity ~99.97% at 3 μm) mounted on opposite sides of the main chamber via high-precision alignment tools. The cavity mirrors are protected from plasma contaminations by special N_2 curtains in front of the reflective surface of each mirror.

The idler output of a commercial single-frequency single-mode continuous wave optical parametric oscillator (cw-OPO, Aculight, Argos 2400-SF-B), operating at ~3 μm with an output power of ~1.2 W and a bandwidth of <1 MHz, is employed as infrared light source. The infrared beam is led through an acousto-optical modulator (AOM), and the first-order deflection (~5%), is spatially filtered by a two-lens telescope system configured with a 150 μm pinhole and then coupled to the ring-down cavity. The cavity length is modulated at 20 Hz by applying a periodic triangle voltage to a piezo-electric transducer mounted on one of the mirror holders. The modulation amplitude is selected to ensure that the cavity is in resonance with the infrared laser at least twice in one period. A hardware (boxcar integrator) based multi-trigger and timing scheme, which has been recently described in detail in Ref. [48], is used to coincide each plasma pulse to one ring-down event. Typical ring-down times are ~5 μs, corresponding to ~3000 effective passes through the planar plasma jet.

An absorption spectrum is recorded by measuring ring-down times as a function of infrared laser frequency. The full experimental spectrum presented in this paper was recorded over 3 weeks. The laser frequency is simultaneously calibrated using a wavelength meter (Bristol Instruments, 621A-IR, self-calibrated by a stabilized He–Ne laser) which provides relative and absolute frequency accuracies better than 6 MHz and 20 MHz, respectively. The frequency calibration is independently checked by recorded absorption features of the precursor C_2H_2 and trace H_2O molecules in the vacuum chamber, indicating a precision of the absolute infrared frequency over one month better than 30 MHz. It should be noted that, when extracting the line positions from our experimental spectra, due to the dense spectral features and heavy line blending, the accuracy of line position determinations for weak and/or heavily blended transitions may be slightly worse, but is still believed to be better than 45 MHz.

3. Results and discussion

3.1. Experimental spectra

Fig. 1 shows an overview of our experimental spectrum in the 3306–3342 cm^{-1} region. A small part of the experimental spectra at ~3330 cm^{-1} was already shown in Ref. [48]. Previous experimental work [35,36,38] and theoretical predictions [49,50] showed that this region is characteristic of the C—H stretch vibrations (both symmetric and asymmetric) of polyacetylenes. As indicated in Fig. 1, strong and spectrally contaminating absorption features due to the precursor C_2H_2 molecules can be easily discriminated based on the line list available in the HITRAN database [51]. Two spectral forests are clearly visible in the 3325–3340 cm^{-1} and 3308–3320 cm^{-1} regions. Based on previous room-temperature FTIR work on HC_4H and HC_6H [38,47,52,53], the former corresponds to the region of the C—H asymmetric stretch (e.g., ν_4 of HC_4H, and ν_5 of HC_6H) fundamental and associated hot bands of polyacetylenes, and the latter corresponds to the region of the C—H symmetric stretch (e.g., ν_1 of HC_4H, and likely HC_6H) associated hot bands.

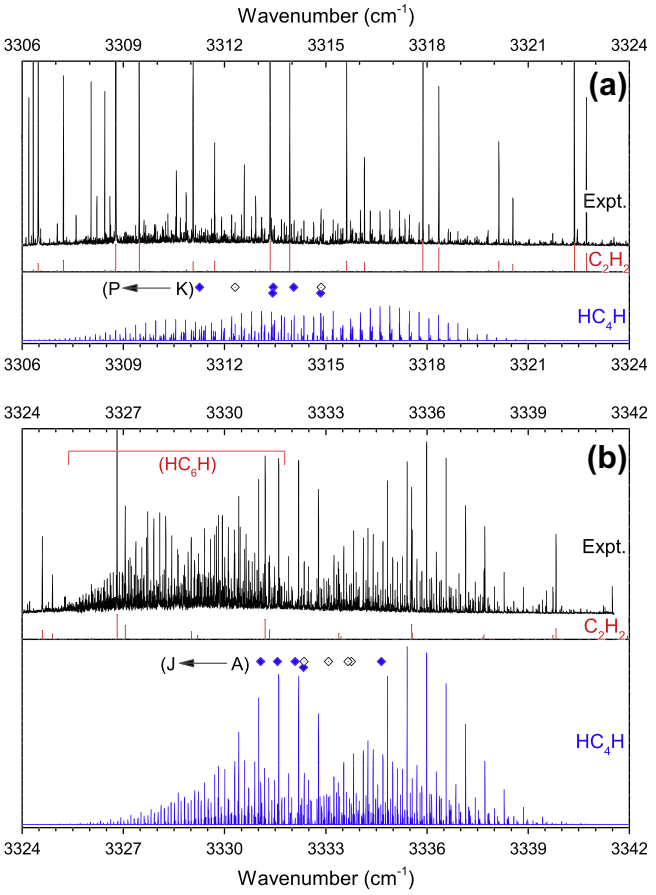

Fig. 1. In both panels, upper trace: an overview of the experimental spectra recorded through a supersonic hydrocarbon plasma jet; middle trace, C_2H_2 lines available from the HITRAN database; lower panel: simulated sum spectrum of the sixteen observed bands of HC_4H, using the spectroscopic parameters and relative level populations as listed in Table 2. Band origins are marked by empty and filled diamond symbols for previously reported and newly observed bands, respectively. The spectral region of the strong HC_6H ν_5 fundamental band is marked in panel (b). (A color version of this figure is available online).

Our preliminary analysis [48] has shown that, even in a supersonic jet where the rotational temperature is only ~17 K, more than 2000 lines are recorded, including a series of strong vibrational hot bands of HC_4H and HC_6H. This paper will focus on the analysis of the observed vibrational bands of HC_4H, specifically the hot band transitions which provide spectroscopic information of vibrationally excited HC_4H. The HC_6H data will be discussed in a separate paper.

To assist the following analysis and discussion, a summary of the nine normal vibrational modes of HC_4H as available from literature is given in Table 1.

3.2. Spectral analysis

The preliminary analysis shows that, at least sixteen separate bands of HC_4H can be recognized in our experimental spectrum. Their band origins are marked by diamond symbols in Fig. 1. Here we label the sixteen bands by capital letters A, B, up to P in a descending order of infrared frequencies of their band origins, as indicated in Fig. 1 and Tables 2 and 3. The determined line positions and corresponding rotational assignments from our analysis are given in Supplementary material. In this spectral region, the ν_4 fundamental band, 4_0^1 (C), and six hot bands, $4_0^1 6_1^1$ (B), $4_0^1 9_1^1$ (D), $4_0^1 9_2^2$, $4_0^1 7_1^1$ (E), $1_0^1 8_0^1 6_1^0$ (J), and $1_0^1 6_0^1 8_1^0$ (O), have been previously measured at room temperature, and analyzed by Guelachvili et al. [38]. Among these previously reported bands, only the $4_0^1 9_2^2$ band is too weak to be unambiguously identified in our spectra. A comparison of line positions measured in the present work to those reported in Ref. [38] shows good agreement, with deviations for most strong and fully resolved lines smaller than 5×10^{-4} cm^{-1}. The only exception is the 4_0^1 fundamental (i.e., the CH asymmetric stretch) band, in which some lower-J transition lines ($10 < J < 25$) show a small shift of about -8×10^{-4} - cm^{-1} (rms) with respect to the data reported in Ref. [38]. The origin of this small, but systematic, offset is unclear as it is not found for other bands (e.g., the $4_0^1 6_1^1$ hot band) in the same wavenumber range.

Table 1
A summary of the normal vibrational modes of HC_4H.

Mode	Vibration	Wavenumber (cm^{-1})		Vib-rot constant (10^{-4} cm^{-1})	
		ω[a]	v[b]	α (*Ab initio*)[c]	α (Expt.)
ν_1 (σ_g^+)	C—H stretch	3489	3332.15	2.167	2.153(10)[d]
ν_2 (σ_g^+)	C≡C stretch	2222	2188.93	6.552	–
ν_3 (σ_g^+)	C—C stretch	885	871.96	3.134	1.03[e], 3.110(deperturbed)[c]
ν_4 (σ_u^+)	C—H stretch	3490	3333.66	2.170	2.191[f], 2.183(4)[d]
ν_5 (σ_u^+)	C≡C stretch	2050	2022.24	3.911	3.948[b]
ν_6 (π_g)	H—C≡C bending	638	625.64	−0.825	−0.678[e]
ν_7 (π_g)	C≡C—C bending	490	482.71	−2.786	−2.711[g]
ν_8 (π_u)	H—C≡C bending	641	628.04	−0.714	−0.636[e]
ν_9 (π_u)	C≡C—C bending	223	220.12	−4.194	−4.183[g]

[a] The estimated empirical harmonic vibrational wavenumbers, taken from Ref. [54].
[b] Experimental vibrational fundamental vibrational wavenumbers, taken from Ref. [38].
[c] Ref. [50].
[d] Constrained values in this work.
[e] Ref. [36].
[f] Ref. [38].
[g] Ref. [44].

Table 2
Lower-state spectroscopic parameters (in cm^{-1}) of the observed sixteen infrared bands of HC_4H.[a]

Band	Assignment	B″	$q'' * 10^5$	$D'' * 10^8$	$q_D'' * 10^{10}$	$H'' * 10^{15}$	G_v''	Relative population[f]
A	(4_0^1? $\Sigma_g^+ - \Sigma_u^+$)	0.146326(11)		1.6[c]				0.08
	(4_0^1? $\Sigma_u^+ - \Sigma_g^+$)	0.1461157(89)		1.6[c]				
B[b]	$4_0^1 6_1^1$ Π_u–Π_g	0.14647893	−8.2895	1.57471	3.96	1.09	625.64[d]	0.28
C[b]	4_0^1 $\Sigma_u^+ - \Sigma_g^+$	0.146411184		1.56825			0	1
D[b]	$4_0^1 9_1^1$ Π_g–Π_u	0.14682982	−20.532	1.6288	4.289		219.97[d]	0.16
E	$4_0^1 7_1^1$ Π_u–Π_g	0.1466788(24)	−12.15(23)	1.572(31)	10		482.71[d]	0.68
F	(4_0^1? Π_g–Π_u)	0.1467387(98)	−8(2)	1.6[c]				0.10
G	(4_0^1? Π_u–Π_g)	0.146537(12)	−3.3(24)	1.6[c]				0.09
H	$4_0^1 8_1^1$ Π_g–Π_u	0.14647473	−8.0374	1.5748	0.437	1.087	628.04[d]	0.28
I	$4_0^1 7_2^2$ Δ_u–Δ_g	0.1469769(53)	$-5.3(16) * 10^{-3}$	1.6[c]			962.96[d]	0.24
J[b]	$1_0^1 8_0^1 6_1^0$ Π_u–Π_g	0.14647893	−8.2895	1.57471	3.96	1.09	625.64[d]	0.28
K	$1_0^1 8_0^1 6_2^1$ Δ_u–Δ_g	0.1465790(58)		1.6[c]			1290.4[e]	0.068
L	$1_0^1 8_0^1 6_2^1$ $\Sigma_u^+ - \Sigma_g^+$	0.1465464(13)		1.539(28)			1283.2[e]	0.035
M	$1_0^1 8_0^1 6_1^0 7_1^1$ Δ_u–Δ_g	0.1467396(46)	$-3.0(26) * 10^{-3}$	1.6[c]			1144.8[e]	0.045
N	$1_0^1 8_0^1 6_2^1 7_1^1$ Φ_u–Φ_g	0.1467848(79)		1.6[c]			1799.6[e]	0.023
O[b]	$1_0^1 6_0^1 8_1^0$ Π_g–Π_u	0.14647473	−8.0374	1.5748	0.437	1.087	628.04[c]	0.28
P	$1_0^1 6_0^1 8_1^0 7_1^1$ Δ_g–Δ_u	0.1467568(31)	−0.0208(13)	1.6[c]			1138.1[e]	0.089

[a] The numbers in parentheses are one standard deviation.
[b] Lower-state molecular constants fixed to the values available from Ref. [36].
[c] Fixed in the fit.
[d] Ref. [38].
[e] Calculated values using the *ab initio* predicted vibrational anharmonicity constants in Ref. [50].
[f] Normalized to the ground-state population (see text).

Table 3
Upper-state spectroscopic parameters (in cm^{-1}) of the observed sixteen infrared bands of HC_4H.[a]

Band	Transition	T_v	B'	$q' * 10^5$	$D' * 10^8$	$q'_D * 10^{10}$
A	$(4_0^1? \Sigma_g^+ - \Sigma_u^+)$	3334.6481(2)	0.1461121(95)		1.6[b]	
	$(4_0^1? \Sigma_u^+ - \Sigma_g^+)$	3334.9403(2)	0.1459024(77)		1.6[b]	
B	$4_0^1 6_1^1 \Pi_u$–Π_g	3333.7562(1)	0.1462554(2)	−8.05(3)	1.570(4)	1.3(7)
C	$4_0^1 \Sigma_u^+ - \Sigma_g^+$	3333.6634(1)	0.1461929(4)		1.506(24)	
D	$4_0^1 9_1^1 \Pi_g$–Π_u	3333.0862(1)	0.1466149(6)	−20.56(6)	1.628(41)	4.29[b]
E	$4_0^1 7_1^1 \Pi_u$–Π_g	3332.3632(1)	0.1464595(23)	−12.04(23)	1.572(31)	8.6(5)
F	$(4_0^1? \Pi_g$–$\Pi_u)$	3332.3429(3)	0.1466006(98)	−6(2)	1.6[b]	
G	$(4_0^1? \Pi_u$–$\Pi_g)$	3332.0975(2)	0.146313(11)	−2.5(22)	1.6[b]	
H	$4_0^1 8_1^1 \Pi_g$–Π_u	3331.5727(2)	0.1462642(15)	−7.38(19)	1.6[b]	
I	$4_0^1 7_2^2 \Delta_u$–Δ_g	3331.0740(2)	0.1467864(15)	$-2.8(16) * 10^{-3}$	5.31(76)	
J	$1_0^1 8_0^1 6_1^0 \Pi_u$–Π_g	3314.8618(2)	0.1462622(3)	−8.58(4)	1.584(8)	1.3(14)
K	$1_0^1 8_0^1 6_2^1 \Delta_u$–$\Delta_g$	3314.8528(3)	0.1463880(14)	−0.002[b]	1.6[b]	
L	$1_0^1 8_0^1 6_2^1 \Sigma_u^+ - \Sigma_g^+$	3314.0531(2)	0.1463374(42)		2.799(386)	
M	$1_0^1 8_0^1 6_1^0 7_1^1 \Delta_u$–$\Delta_g$	3313.4415(2)	0.1465373(46)	$-4.6(26) * 10^{-3}$	1.6[b]	
N	$1_0^1 8_0^1 6_2^1 7_1^1 \Phi_u$–$\Phi_g$	3313.4344(2)	0.1465843(77)		1.6[b]	
O	$1_0^1 6_0^1 8_1^0 \Pi_g$–Π_u	3312.3136(2)	0.1462609(7)	−8.46(2)	1.484(32)	
P	$1_0^1 6_0^1 8_1^0 7_1^1 \Delta_g$–$\Delta_u$	3311.2618(1)	0.1465414(92)	$-1.64(12) * 10^{-2}$	1.6[b]	

[a] The numbers in parentheses are one standard deviation.
[b] Fixed in the fit.

All bands observed in the present work are parallel transitions, i.e., the quantum number l, related to the projection of the total vibrational angular momentum on the symmetry axis, does not change upon vibrational excitation. In total, four types of vibrational transitions are observed: Σ–Σ, Π–Π, Δ–Δ, and Φ–Φ, corresponding to l = 0, 1, 2, and 3, respectively. The Σ–Σ type bands, including the ν_4 fundamental band, consist of simple P- and R-branches, and exhibit 3:1 line intensity alternations in each branch due to nuclear spin statistics for lower-state rotational levels with different parity facilitated even-/odd-J numbering. The other three band types with $l \neq 0$ are degenerated due to rotational l-type doubling, i.e., each rotational line comprises two components with a relative intensity ratio of 3:1/1:3 which are only resolved for some high-J transitions. Moreover, for the $l \neq 0$ bands, weak and unresolved or partially resolved Q-branches (Fig. 2) are also observed, with intensities relative to P-/R- branch transitions (in the same band) proportional to l^2.

The rotational analysis of each band is performed in the PGOPHER software [55], starting from a standard ro-vibrational Hamiltonian for linear molecules:

$$\mathbf{H} = \mathbf{H}_{vib} + B\mathbf{N}^2 - D\mathbf{N}^4, \quad (1)$$

which gives the following expression of ro-vibrational energy levels (v, l, J)

$$E(v,l,J) = G_{v,l} + B_v[J(J+1) - l^2] - D_v[J(J+1) - l^2]^2, \quad (2)$$

where $\mathbf{H}_{vib}$ is the vibrational Hamiltonian, $\mathbf{N}$ the rotational angular momentum, $G_{v,l}$ the vibrational energy, B_v the rotational constant, and D_v the quartic centrifugal distortion constant, respectively. For the v_6 = 1 and v_8 = 1 levels, accurate sextic centrifugal distortion constants, $H_{(v)}$, corresponding to the $H\mathbf{N}^6$ term in the total Hamiltonian, are available from submillimeter-wave data, and are consequently included in our analysis. For the $l \neq 0$ degenerated vibrational levels, the rotational l-type doubling is demonstrated by the off-diagonal term:

$$q/2 * (N_+^{(2l)} L_-^{(2l)} + N_-^{(2l)} L_+^{(2l)}) \quad (3)$$

where q is the rotational l-type doubling constant, and $\mathbf{L}$ the vibrational orbital angular momentum.

For the Π–Π (l = 1) type (B), (H), (J), and (O) bands, high-J transition lines have been previously reported in Ref. [38], and the rotational analysis here is performed by combining the low-J transition data in our jet-cooled spectra, and high-J transition data available from Ref. [38], with inclusion of the centrifugal distortion term of the rotational l-type doubling:

$$q_D/4[\mathbf{N}^2, (N_+^2 L_-^2 + N_-^2 L_+^2)]_+ \quad (4)$$

It should be noted that the parameters q and q_D used here correspond to $-q_t$, and $-q_{tJ}$ used in Refs. [35,36], respectively, due to a different definition of the signs in our analysis.

Vibrational assignments of the nine new bands are made based on the vibration–rotation interaction constants of lower and upper states of each band. The vibration–rotation interaction constant (α_i) is given by:

$$B_v = B_e + \Sigma_i[\alpha_i(v_i + d_i/2)] = B_0 + \Sigma_i(\alpha_i v_i) \quad (5)$$

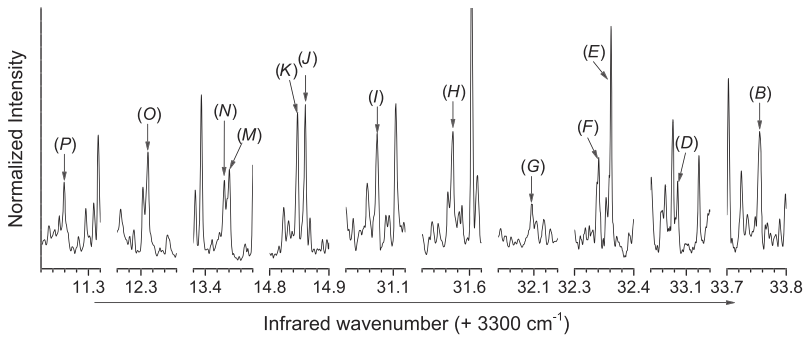

Fig. 2. The weak Q branches (indicated by arrows, and band labels as in Tables 1 and 2) of the observed degenerated transition bands of HC_4H.

where i represents the vibrational quantum numbers, d_i is the degree of the degeneracy of the v_i mode with vibrational quantum number v_i (see Table 1), and B_e the equilibrium rotational constant. As higher order terms are neglected, calculations using Eq. (5) may cause relatively large deviations, particularly for highly excited vibrational combination levels. In practice, the variant of Eq. (5) that is used in our analysis is given by:

$$B_{(j+i)} = B_j + \alpha_i * v_i \quad (6)$$

where j represents a well-established vibrational level, $(i+j)$ the vibrational combination level of level j and another vibrational mode v_i. In Table 1, also the available values of α_i for each vibrational mode of HC_4H are summarized. It can be seen that the *ab initio* predicted values for α_3, α_4, α_5, α_7, and α_9 in Ref. [50] are in good agreement with previously reported (deperturbed) experimental values, i.e., within 1%, while α_6 and α_8 show larger deviations (>10%). Therefore, the experimental values for α_6 and α_8, and the *ab initio* predicted values for other modes are used in the analysis of newly observed vibrational combination levels.

Spectral analyses of the nine new bands are performed as follows. The line positions in each band determined in the present work are interpreted in preliminary fits with inclusion of parameters T_v, B' and B'' only, to derive a set of tentative rotational constants. Two types of fits are employed for each band: by fitting the transition frequencies directly, and by fitting lower- and upper-state combination differences. In general, the two routines give very similar spectroscopic parameters, except for one case in which the upper-state level is significantly perturbed. It should be noted that the combination difference fit does not result in band origin values (T_v). The resulting rotational constants (B' and B'') are consequently used to calculate the corresponding vibration–rotation interaction constants (α_i) by Eq. (6), which yields tentative vibrational assignments for most of the new bands. The vibrational assignments of all observed bands are summarized in Table 2. With the vibrational assignments done, systematic rotational analyses on all observed bands are carried out in combination with previous submillimeter-wave and infrared data [35,36,38,44,45]. The details for the individual bands are discussed below. The resulting spectroscopic parameters are summarized in Tables 2 and 3.

3.2.1. 4_0^1 ($\Sigma_u^+ - \Sigma_g^+$) fundamental band (C)

The 4_0^1 fundamental band (C) at ~3333.66 cm^{-1}, is the strongest band of HC_4H in this region. As mentioned above, some transition lines ($10 < J < 25$) determined in our experiment show a small systematic shift ($\sim -8 \times 10^{-4}$ cm^{-1}, rms) compared to data in Ref. [38]. Since this shift is not found in other hot bands, and is within the uncertainties of the absolute infrared frequency in both studies, no corrections are made when combining our low-J spectral data with the high-J spectral data in Ref. [38].

A lower-state combination difference fit of all available data results in ground-state constants of $B_0 = 0.1464123(17)$ and $D_0 = 1.563(22) \times 10^{-8}$ cm^{-1}. The inclusion of the sextic centrifugal distortion term does not improve this fit. The values are in good agreement with the most accurate values currently available from Ref. [36], of $B_0 = 0.146411184(20)$ and $D_0 = 1.56825(20) \times 10^{-8}$ cm^{-1}. This confirms the reliability of our approach to combine our experimental data with those in Ref. [38]. As heavy rotational perturbations for $J' > 45$ upper-state levels have been found in the previous study [38], the upper state constants listed in Table 3 are obtained by fixing B_0 and D_0 to the values in Ref. [36] and fitting $J' \leqslant 45$ unperturbed transitions only. The derived $\alpha_4 = 2.183(4) \times 10^{-4}$ cm^{-1} is very close to the *ab initio* predicted value, with a deviation (~0.5%) similar as for α_3 and α_9 [36,50].

3.2.2. $4_0^1 6_1^1$ (B) and $1_0^1 8_0^1 6_1^0$ (J) Π_u–Π_g bands

Bands (B) and (J) have the same $v_6 = 1$ (Π_g) lower state, whose spectroscopic parameters have been accurately determined previously by Bizzocchi et al. [35,36], and thus are fixed in the fits. All the ro-vibrational lines of both bands determined in the present work and in Ref. [38] can be well fitted, resulting in effective upper-state spectroscopic parameters as summarized in Table 3.

It is noted that the two upper vibrational levels, $4^1 6^1$ and $1^1 8^1$, are of the same Π_u symmetry, with similar vibrational energies. It is principally possible that the two upper levels interact via Fermi resonance. However, the experimentally determined $\alpha_{(4+6)} = 1.558(2) \times 10^{-4}$ cm^{-1}, and $\alpha_{(1+8)} = 1.510(3) \times 10^{-4}$ cm^{-1}, are only ~3% different from the predicted values of $(\alpha_4 + \alpha_6)$ and $(\alpha_1 + \alpha_8)$ in Table 1. This indicates that the Fermi resonance between the $4^1 6^1$ and $1^1 8^1$ levels should be very small and can be neglected, if it exists.

3.2.3. $4_0^1 8_1^1$ (H) and $1_0^1 6_0^1 8_1^0$ (O) Π_g–Π_u bands

The $1_0^1 6_0^1 8_1^0$ band has been reported by Guelachvili et al. [38], but the $4_0^1 8_1^1$ hot band was not identified in Ref. [38] due to heavy spectral overlapping in the room-temperature spectrum. Among the newly observed bands in our spectrum, a relatively strong band, (H) at ~3331.57 cm^{-1}, is found to have a lower state with a tentative rotational constant B''~0.14648 cm^{-1} and a Π_u level symmetry that both are consistent with the $v_8 = 1$ level. The vibration–rotation interaction constants (α_i) calculated from both lower- and upper-state rotational constants with respect to the 4_0^1 band are found to be $\sim 0.8(1) \times 10^{-4}$ cm^{-1}, comparable to α_8. Therefore, the band (H) is assigned to the $4_0^1 8_1^1$ hot band transition.

The two bands, $4_0^1 8_1^1$ (H) and $1_0^1 6_0^1 8_1^0$ (O), have the same $v_8 = 1$ (Π_u) lower state. The spectroscopic parameters of the $v_8 = 1$ level have been accurately determined by Bizzocchi et al. [35], and are fixed in our fit. Similar as discussed in Section 3.2.2, no significant Fermi-type rotational perturbations are found for the two upper vibrational states, $4^1 8^1$ and $1^1 6^1$. The room-temperature spectrum of the $1_0^1 6_0^1 8_1^0$ band in Ref. [38] shows a heavy perturbation for $24 < J' < 37$ transition lines. Our analysis indicates that this perturbation is not due to an interaction between the $4^1 8^1$ and $1^1 6^1$ levels, and must be caused by other dark states lying around this vibrational energy region. Actually, when analyzing the jet-cooled spectrum of the $4_0^1 8_1^1$ band, perturbations seem to show up for $J' > 17$ transitions, but these spectral lines are too weak for an unambiguous identification. As such, the rotational assignments and the fit of the $4_0^1 8_1^1$ (H) band are only made for $J' \leqslant 17$. For the $1_0^1 6_0^1 8_1^0$ band, the perturbed lines with $25 < J' < 37$ are excluded from the fit.

3.2.4. $4_0^1 9_1^1$ (D) Π_g–Π_u band

In the previous room-temperature study [38], the $4_0^1 9_1^1$ band is the strongest hot band in this region, but heavy spectral overlapping with the 4_0^1 fundamental band only allows for unambiguously assigning some P-branch transitions of the e component. In our jet-cooled spectra, this band is relatively weak. The reduced Doppler width and low rotational temperature, however, allow the assignment of low-J transitions of both e and f components. To obtain upper-state spectroscopic parameters, the parameters for the lower $v_9 = 1$ level are fixed to values available from Ref. [36], and the perturbed P($J > 42$) lines in the room-temperature spectrum [38] are not included in the fit.

3.2.5. $4_0^1 7_1^1$ (E) Π_u–Π_g band

The $4_0^1 7_1^1$ band is the second strongest hot band in our jet-cooled spectra. Rotational analysis of this band is performed in combination with the room-temperature data from Ref. [38]. No significant rotational perturbations are found in our analysis. The

resulting spectroscopic parameters for the lower $v_7 = 1$ level, both by fitting the combination differences and by fitting the regular transition frequencies, are in good agreement with the values available from Ref. [44], which are the most accurate values currently so far.

3.2.6. $4_0^1 7_2^2$ (I) Δ_u–Δ_g band

The band (I) at ~3331.07 cm^{-1}, with a profile intensity comparable to the bands $4_0^1 6_1^1$ (B) and $4_0^1 8_1^1$ (H), has not been reported before. Rotational progressions in P- and R-branches of this band starting from P(3) and R(2) are found, as well as a Q-branch that is stronger than in a typical Π–Π band. These traits are consistent with a Δ–Δ ($l = 2$) type transition with characteristic rotational energy ladders in both states starting from $J = 2$, and a Q-branch intensity that is about four times stronger than in a Π–Π type band. The signs of the l-type doubling constants q obtained from the rotational analysis determine the symmetry properties of g and u for lower and upper levels, respectively. The effective values of α of both lower and upper levels with respect to the 4_0^1 fundamental band are $\sim 5.7(1) \times 10^{-4}$ cm^{-1}, about two times α_7. Therefore, this band is assigned to the $4_0^1 7_2^2$ Δ_u–Δ_g transition. The resulting lower- and upper-state spectroscopic parameters are summarized in Tables 2 and 3.

The $4_0^1 7_2^2$ $\Sigma_u^+ - \Sigma_g^+$ component is not found in our spectra, although it is expected to be close to band (I). This may be due to the strong Fermi resonance between the 7_2 (Σ_g^+), 3_1 (Σ_g^+) and $8_1 9_1$ (Σ_g^+) levels [36]. As will be discussed in Section 3.3, the $8_1 9_1$ (Σ_g^+) level involving an excitation of the v_9 mode, cannot be efficiently populated in our plasma source. Therefore, this three-state Fermi resonance system may cause the $4_0^1 7_2^2$ $\Sigma_u^+ - \Sigma_g^+$ component to be below our detection limit.

3.2.7. (M) Δ_u–Δ_g and $1_0^1 6_0^1 8_1^0 7_1^1$ (P) Δ_g–Δ_u bands

Similar as for band (I) discussed in Section 3.2.6, the two new bands, (M) and (P) with band origins at ~3313.44 and 3311.26 cm^{-1}, respectively, are identified as Δ–Δ type transitions. The rotational constants of the two bands, for both lower and upper states, are found to be about 2.8×10^{-4} cm^{-1} larger than the corresponding values of the $1_0^1 8_0^1 6_1^0$ Π_u–Π_g (J) and $1_0^1 6_0^1 8_1^0$ Π_g–Π_u (O) bands. This difference is nearly the same as the vibration–rotation interaction constant α_7. Therefore, the bands (M) and (P) are assigned to $1_0^1 8_0^1 6_1^0 7_1^1$ Δ_u–Δ_g and $1_0^1 6_0^1 8_1^0 7_1^1$ Δ_g–Δ_u transitions, respectively. Although the errors of the l-type doubling constants q in our fits are slightly larger, the derived signs of q are consistent with the different lower-state symmetry properties of $6_1 7_1$ (Δ_g) and $8_1 7_1$ (Δ_u). As the lower states of both bands have not been reported before, all spectroscopic parameters (lower- and upper-state) of both bands listed in Tables 2 and 3 are determined directly from our jet-cooled spectrum.

3.2.8. $1_0^1 8_0^1 6_2^1$ Δ_u–Δ_g (K), $1_0^1 8_0^1 6_2^1$ $\Sigma_u^+ - \Sigma_g^+$ (L) and $1_0^1 8_0^1 6_2^1 7_1^1$ (N) Φ_u–Φ_g bands

Two weak bands, (K) and (N), are found very close to $1_0^1 8_0^1 6_1^0$ Π_u–Π_g (J), and $1_0^1 8_0^1 6_1^0 7_1^1$ Δ_u–Δ_g (M), respectively. The weak Q-branches of (K) and (N) are found to be only ~0.01 cm^{-1} lower than (J) and (M), respectively. A preliminary analysis indicates that (K) and (N) are due to Δ–Δ and Φ–Φ transition types, i.e., with the same increase of l by 1 with respect to bands (J) and (M), respectively. Most assigned rotational lines in the two bands are relatively weak, and the corresponding rotational l-type doubling constants could not be determined. The vibrational assignments of $1_0^1 8_0^1 6_2^1$ Δ_u–Δ_g for band (K) and $1_0^1 8_0^1 6_2^1 7_1^1$ Φ_u–Φ_g for band (N), are made based on the derived rotational constants and vibration–rotation interaction constants only. It should be noted that, in the $1_0^1 8_0^1 6_2^1$ Δ_u–Δ_g (K) band, weak local perturbations are found for $J' < 3$ transitions, which cause a disagreement between the Q-branch peak position and the band origin derived from fitting the P- and R-branches. The lower-state parameters for band (K) in Table 2 are thus obtained from a combination difference fit, while the upper-state parameters in Table 3 are obtained with exclusion of the $J' < 5$ perturbed lines in the fit.

In addition, a Σ–Σ type band (L) is found at ~3314.05 cm^{-1}, with a corresponding lower state symmetry/parity property of $g/+$ or $u/-$. The estimated vibration–rotation interaction constants from the fit indicate that an excitation of the v_7 or v_9 mode is not involved. As the vibration–rotation interaction constants α_6 and α_8 are very close, the present data does not allow us to determine rotational constants accurate enough to identify the corresponding vibrational assignment. The relative population in the lower state of bands (L) and (K), as will be discussed in detail below, is estimated to be ~1:2, which is consistent with degeneracies of Σ and Δ vibrational levels. Thus, with this additional information, band (L) is assigned to the $l = 0$ $\Sigma_u^+ - \Sigma_g^+$ component of the $1_0^1 8_0^1 6_2^1$ transition.

3.2.9. Unassigned bands A, F, and G

Three weak bands, (A), (F) and (G), are found in the v_4 hot band region. The estimated $(B'-B'')$ values of all three bands are $\sim 2.18(4) \times 10^{-4}$ cm^{-1}, and are nearly the same as α_4, indicating that these bands are due to 4_0^1 associated hot band transitions. The tentative rotational assignments of the three bands are given in Supplementary material. Band (A) at ~3334.9 cm^{-1} is found to be a Σ–Σ type transition, since the 3:1 line intensity alternations in both P- and R-branches are clearly seen. Spectral overlap prohibits the identification of the weak P(1) and R(0) lines and the determination of lower-state symmetry/parity properties, and consequently no unambiguous rotational assignment can be made. Two different fits are tried by assuming that the lower state is Σ_g^+ or Σ_u^+. Effective lower-state vibration–rotation interaction constants $\alpha \sim 2.9 \times 10^{-4}$ cm^{-1} for the Σ_g^+ case and $\sim 0.9 \times 10^{-4}$ cm^{-1} for the Σ_u^+ case are obtained. The positive value of α indicates that the excitation of at least one stretch vibration mode is involved in the lower state, likely the v_3 (σ_g) mode with the lowest stretch vibrational energy. A possible assignment of the lower state of band (A) is the 3_2 (Σ_g^+) level perturbed by other nearby Σ_g^+ levels, or a complex vibrational combination level of v_3 and other bending modes.

The bands (F) and (G) at ~3332.34 and 3332.10 cm^{-1}, respectively, are heavily overlapped with other bands. The estimated rotational constants and vibration–rotation interaction constants seem to be consistent with lower-state assignments of $7_1 6_1$ (Δ_g) and a 6_2 (Δ_g) for bands (F) and (G), respectively. The relative intensities of weak Q-branches and tentatively assigned R(1) and P(2) transitions in our spectrum (see Supplementary material) indicate that both bands are likely due to Π–Π type transitions. In Tables 2 and 3, spectroscopic parameters are listed based on a tentative Π–Π type assignment in the fit.

In the analysis described above, possible perturbations caused by Fermi resonances or Coriolis couplings are not included. Previous work [36] has shown that, even for some low-lying vibrational levels in the 900 cm^{-1} region, heavy perturbations in the Fermi resonance system of 7_2 (Σ_g^+), 3_1 (Σ_g^+) and $8_1 9_1$ (Σ_g^+) levels are found. The vibrational bands analyzed in this work have lower and upper state vibrational energies in the 0–1800 and 3300–5100 cm^{-1} range, respectively, and thus Fermi-resonance or Coriolis-coupling type perturbations between occasionally nearby vibrational levels may occur. The rotational analyses presented here, and in Ref. [38] indicate that some of these bands exhibit significant heterogeneous perturbations by one or more perturbers. The present experimental dataset, although extensive, does not allow performing a full deperturbation analysis of these specific features at this stage. For this, more accurate measurements of these excited vibrational

levels in this wavelength region are needed, as well as an extension of the present data to other IR wavelength regions.

3.3. Vibrational excitation temperatures

In the previous room-temperature spectra [38], the relative band intensities of the 4_0^1 associated hot bands follow the order of $4_0^1 9_1^1 > 4_0^1 9_2^2 > 4_0^1 7_1^1 > 4_0^1 6_1^1 \sim 4_0^1 8_1^1$, which agrees well with the Boltzmann factors estimated from the corresponding lower-state vibrational energies. However, in our plasma jet-cooled spectrum these relative band intensities are rather different, and the order of the intensity of the 4_0^1 associated hot bands becomes: $4_0^1 7_1^1 > 4_0^1 6_1^1 \sim 4_0^1 8_1^1 > 4_0^1 7_2^2 > 4_0^1 9_1^1$. It should be noted that the rotational temperature of all HC_4H bands in our spectra is found to be only ~17(1) K, which is substantially lower than the vibrational excitation temperature in our plasma jet source. To evaluate the non-Boltzmann populations of HC_4H in its low-lying vibrational levels in the plasma jet expansion, the relative molecular populations in the lower states of the sixteen observed bands are estimated as follows:

(1) We assume that the transition dipole moments of all 4_0^1 associated hot bands are the same as for the 4_0^1 fundamental transition, i.e., the bands (A–I) have of the same transition strength $S(4_0^1)$. Similarly, the bands (J–N) have a transition strength $S(1_0^1 8_0^1 6_1^0)$, and the bands (M) and (N) follow $S(1_0^1 6_0^1 8_1^0)$.

(2) The intensities of the bands $4_0^1 6_1^1$ (B) and $1_0^1 8_0^1 6_1^0$ (J) Π_u–Π_g which have the same lower vibrational level, are used to estimate the $S(4_0^1)/S(1_0^1 8_0^1 6_1^0)$ ratio as ~0.45(3). Similarly, the $S(4_0^1)/S(1_0^1 6_0^1 8_1^0)$ ratio is estimated to be ~1.27(5) from the bands $4_0^1 8_1^1$ (H) and $1_0^1 6_0^1 8_1^0$ (O).

The estimated relative lower-state populations from our spectra shown in Fig. 1 are listed in Table 2, where the numbers are normalized to the ground-state population derived from the 4_0^1 band. It should be noted that the full spectrum shown in Fig. 1 was measured over a period of three weeks, and some small daily fluctuations in the exact discharge conditions may affect the absolute spectral line intensities. Therefore, our estimate relies mainly on the overall pattern of relatively strong P(J) and R(J) lines ($2 < J < 12$), which cover more than 7 cm^{-1} range in each band. The error in the population values listed in Table 2 is estimated to be smaller than 20%. A simulated sum spectrum of HC_4H using the derived spectroscopic parameters and lower-state populations of all sixteen observed bands is shown in Fig. 1, exhibiting a good agreement in overall spectral pattern with the experimental spectrum.

Fig. 3 shows a plot of the normalized molecular populations (in a natural logarithm scale) vs. lower-state vibrational excitation energies. Some of the lower-state vibrational energies were not reported before, and are calculated here using the *ab initio* predicted anharmonicity constants in Ref. [50]. It is found that, in the plasma jet, the population of HC_4H in the $v_9 = 1$ level follows a relatively low vibrational temperature of ~125(10) K, while populations in levels involving excitation of the v_6, v_7 and v_8 vibrational modes follow a much higher vibrational temperature of ~580(50) K. The population in the $6_1 7_1$ level, derived from the $1_0^1 8_0^1 6_1^0 7_1^1$ (M) band, is slightly smaller than the fitted Boltzmann distribution curve (Fig. 3). This may be caused by possible Fermi-resonance type (homogeneous) perturbations which can significantly decrease the transition strength of the $1_0^1 8_0^1 6_1^0 7_1^1$ band. Moreover, the relatively low vibrational temperature for the v_9 mode is also consistent with our experimental observation that, except for the $4_0^1 9_1^1$ band, none of the hot band transitions with lower levels involving an excitation of the v_9 mode are observed in the plasma jet, including the $4_0^1 9_2^2$ band which is the second strongest hot band in the room-temperature spectrum [38].

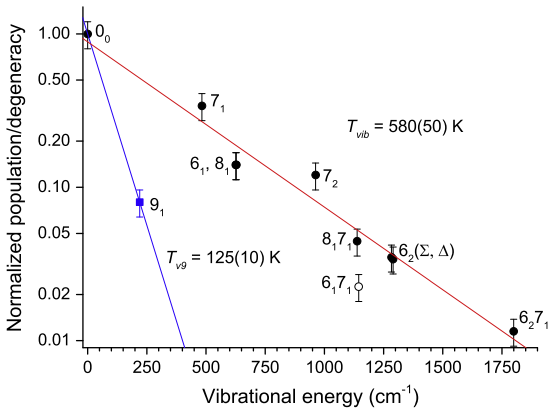

Fig. 3. A plot of the molecular populations (normalized to the ground state, in natural logarithm scale) vs. lower-state vibrational energy of HC_4H in our supersonic jet experiment. The data points for 6_1 and 8_1 levels are too close to be distinguished in the plot.

The non-equilibrium vibrational excitation and relaxation of linear polyatomic molecules in a plasma jet has been discussed in Ref. [56]. Although a different discharge nozzle is used in our experiment, the vibrational excitation of HC_4H shows a similar behavior as that of the linear molecules discussed in Ref. [56]. It is expected that, using our slit discharge nozzle and applying different discharge conditions, other non-polar molecules or radicals in their low-lying vibrational levels up to several hundred cm^{-1} can be produced. Although the hot band spectra complicate the rotational analysis, this also provides an opportunity to derive values for the low-lying vibrational levels of non-polar species, such as polyynes (HC_nH), bare carbon chains (C_n), and their ions, which are important constituents in the interstellar medium, but are radio-silent and cannot be observed directly via their pure rotational spectrum. These species are spectroscopically accessible via infrared-active ro-vibrational transitions in the mid/far-IR and THz region via low-lying bending modes, as has been demonstrated for astronomical detections of HC_4H and C_3 [31,33,57–59].

4. Conclusions

In this work, we presented the high-resolution infrared spectra of diacetylene (HC_4H) in the C—H stretch vibrational region of 3306–3342 cm^{-1}, recorded in a supersonic planar plasma jet. Detailed and systematic rotational analyses of the observed sixteen bands are performed, resulting in spectroscopic parameters for a series of vibrational levels over wide energy regions of 0–1800 and 3300–5100 cm^{-1}.

Acknowledgments

This work is financially supported by a NWO-VICI grant, NOVA, SRON and has been performed within the context of the Dutch Astrochemistry Network.

Appendix A. Supplementary material

Supplementary data associated with this article can be found, in the online version, at http://dx.doi.org/10.1016/j.jms.2013.11.008.

References

[1] T. Henning, F. Salama, Science 282 (1998) 2204–2210.
[2] K.H. Homann, Angew. Chem. Int. Ed. 37 (1998) 2434–2451.

[3] H. Ritcher, J.B. Howard, Prog. Energy Com. Sci. 26 (2000) 565–608.
[4] T. Fujii, M.J. Kareev, J. Appl. Phys. 89 (2001) 2543–2546.
[5] H.C. Thejaswini, A. Majumdar, T.M. Tun, R. Hippler, Adv. Space Res. 48 (2011) 857–861.
[6] H. Shirakawa, Rev. Mod. Phys. 73 (2001) 713–718.
[7] X. Zhao, Y. Ando, Y. Liu, M. Jinno, T. Suzuki, Phys. Rev. Lett. 90 (2003) 187401.
[8] A. Milani, M. Tommasini, M.D. Zoppo, C. Castiglioni, G. Zerbi, Phys. Rev. B 74 (2006) 153418.
[9] T. Ma, Y. Hu, H. Wang, J. Appl. Phys. 104 (2008) 064904.
[10] R.I. Kaiser, Chem. Rev. 102 (2002) 1309–1358.
[11] R.I. Kaiser, A.M. Mebel, Chem. Rev. Soc. 41 (2012) 5490–5501.
[12] X. Gu, Y. Guo, F. Zhang, A.M. Mebel, R.I. Kaiser, Faraday Discuss. 133 (2006) 245–275.
[13] V. Wakelam, I.W.M. Smith, E. Herbst, J. Troe, W. Geppert, H. Linnartz, K. Öberg, E. Rouef, M. Agundez, P. Pernot, H.M. Cuppen, J.C. Loison, D. Talbi, Space Sci. Rev. 156 (2010) 13–72.
[14] J. Kahanpää, K. Mattila, K. Lehtinen, C. Leinert, D. Lemke, Astro. Astrophys. 405 (2003) 999–1012.
[15] S. Glicker, H. Okabe, J. Phys. Chem. 91 (1987) 437–440.
[16] G. Israel, M. Cabane, F. Raulin, E. Chassefière, J.J. Boon, Ann. Geophys. 9 (1991) 1–13.
[17] R.E. Bandy, C. Lakshminarayan, R.K. Frost, T.S. Zwier, Science 258 (1992) 1630–1633.
[18] R.E. Bandy, C. Lakshminarayan, R.K. Frost, T.S. Zwier, J. Phys. Chem. 98 (1993) 5362–5367.
[19] C. Delpech, J.C. Guillemin, P. Paillous, M. Khlifi, P. Bruston, F. Raulin, Spectrochimica Acta. A 50 (1994) 1095–1100.
[20] R.K. Frost, G.S. Zavarin, T.S. Zwier, J. Phys. Chem. 99 (1995) 9408–9415.
[21] E.H. Wilson, S.K. Atreya, Journal of Geophysical Research: Planets (1991–2012) 109 (2004) E06002.
[22] V.G. Kunde, A.C. Aikin, R.A. Hanel, D.E. Jennings, W.C. Maguire, R.E. Samuelson, Nature 292 (1981) 686–688.
[23] T. de Graauw, H. Feuchtgruber, B. Bezard, P. Drossart, T. Encrenaz, D.A. Beintema, Astron. Astrophys. 321 (1997) L13–16.
[24] A. Jolly, A. Fayt, Y. Benilan, D. Jacquemart, C.A. Nixon, D.E. Jennings, Astrophys. J. 714 (2010) 852–859.
[25] G.R. Gladstone, M. Allen, Y.L. Yung, Icarus 119 (1996) 1–52.
[26] F. Shindo, Y. Benilan, J.C. Guillemin, P. Chaquic, A. Jolly, F. Raulin, Planet. Space Sci. 51 (2003) 9–17.
[27] V.G. Kunde et al., Science 305 (2004) 1582–1586.
[28] M. Burgdorf, G. Orton, J. van Cleve, V. Meadows, J. Houck, Icarus 184 (2006) 634–637.
[29] V.S. Meadows, G. Orton, M. Line, M.C. Liang, Y.L. Yung, J. van Cleve, M.J. Burgdorf, Icarus 197 (2008) 585–589.
[30] J. Cernicharo, A.M. Heras, A.G.G.M. Tielens, J.R. Pardo, F. Herpin, M. Guélin, L.B.F.M. Waters, Astrophys. J. Lett. 546 (2001) L123–126.
[31] J. Cernicharo, A.M. Heras, J.R. Pardo, A.G.G.M. Tielens, M. Guélin, E. Dartois, R. Neri, L.B.F.M. Waters, Astrophys. J. Lett. 546 (2001) L127–130.
[32] J.P. Fonfría, J. Cernicharo, M.J. Richter, J.H. Lacy, Astrophys. J. 728 (2011) 43.
[33] A. Evans, V.H. Tyne, J.Th. van Loon, B. Smalley, T.R. Geballe, R.D. Gehrz, C.E. Woodward, A.A. Zijlstra, E. Polomski, M.T. Rushton, S.P.S. Eyres, S.G. Starrfield, J. Krautter, R.M. Wagner, Mon. Not. R. Astron. Soc. 373 (2006) L75–79.
[34] J. Bernard-Salas, E. Peeters, G.C. Sloan, J. Cami, S. Guiles, J.R. Houck, Astrophys. J. Lett. 652 (2006) L29–32.
[35] L. Bizzocchi, C.D. Esposti, L. Dore, Mol. Phys. 108 (2010) 2315–2323.
[36] L. Bizzocchi, F. Tamassia, C.D. Esposti, L. Fusina, E. Cane, L. Dore, Mol. Phys. 109 (2011) 2181–2190.
[37] N.L. Owen, C.H. Smith, G.A. Williams, J. Mol. Struct. 161 (1987) 33–53.
[38] G. Guelachvili, A.M. Craig, D.A. Ramsay, J. Mol. Spectrosc. 105 (1984) 156–192.
[39] K. Matsumura, T. Etoh, T. Tanaka, J. Mol. Spectrosc. 90 (1981) 106–115.
[40] K. Matsumura, T. Tanaka, J. Mol. Spectrosc. 96 (1982) 219–233.
[41] K. Matsumura, K. Kawaguchi, E. Hirota, T. Tanaka, J. Mol. Spectrosc. 118 (1986) 530–539.
[42] K. Matsumura, T. Tanaka, J. Mol. Spectrosc. 116 (1986) 320–333.
[43] K. Matsumura, T. Tanaka, J. Mol. Spectrosc. 116 (1986) 334–350.
[44] D. McNaughton, D.N. Bruget, J. Mol. Struct. 273 (1992) 11–25.
[45] E. Arié, J.W.C. Johns, J. Mol. Spectrosc. 155 (1992) 195–204.
[46] M. Khlifi, P. Paillous, C. Delpech, M. Nishio, P. Bruston, F. Raulin, J. Mol. Spectrosc. 174 (1995) 116–122.
[47] R. Tay, G.F. Metha, F. Shanks, D. McNaughton, Struct. Chem. 6 (1995) 47–55.
[48] D. Zhao, J. Guss, A. Walsh, H. Linnartz, Chem. Phys. Lett. 565 (2013) 132–137.
[49] C. Zhang, Z. Cao, H. Wu, Q. Zhang, Int. J. Quan. Chem. 98 (2004) 299–308.
[50] A.C. Simonett, H.F. Schaefer III, W.D. Allen, J. Chem. Phys. 130 (2009) 044301.
[51] L.S. Rothman et al., J. Quant. Spectrosc. Radiat. Transfer. 110 (2009) 533–572.
[52] D. McNaughton, D.N. Bruget, J. Mol. Struct. 150 (1991) 620–634.
[53] K. Matsumura, K. Kawaguchi, D. McNaughton, D.N. Bruget, J. Mol. Spectrosc. 158 (1993) 489–493.
[54] G.A. Williams, J.N. Macdonald, J. Mol. Struct. 320 (1994) 217–225.
[55] PGOPHER, a Program for Simulating Rotational Structure, C.M. Western, University of Bristol, <http://pgopher.chm.bris.ac.uk>.
[56] M. Eugenia Sanz, M.C. McCarthy, P. Thaddeus, J. Chem. Phys. 122 (2005) 194319.
[57] A. van Orden, J.D. Cruzan, R.A. Provencal, T.F. Giesen, R.J. Saykally, R.T. Boreiko, A.L. Betz, ASP Conf. Ser. 73 (1995) 67–70.
[58] J. Cernicharo, J.R. Goicoechea, E. Caux, Astrophys. J. Lett. 534 (2000) L199–202.
[59] T.F. Giesen, A.O. van Orden, J.D. Cruzan, R.A. Provencal, R.J. Saykally, R. Gendriesch, F. Lewen, G. Winnewisser, Astrophys. J. Lett. 551 (2001) L181–184.